arXiv:0705.3701v3 [astro-ph] 8 Aug 2007

Probing polarization states of primordial gravitational waves with CMB anisotropies

Shun Saito[1], **Kiyotomo Ichiki**[2] **and Atsushi Taruya**[2]

[1] Department of Physics, The University of Tokyo, Tokyo 113-0033, Japan
[2] Research Center for the Early Universe (RESCEU), Graduate School of Science, The University of Tokyo, Tokyo 113-0033, Japan

E-mail: `ssaito@utap.phys.s.u-tokyo.ac.jp`

Abstract. We discuss the polarization signature of primordial gravitational waves imprinted in cosmic microwave background (CMB) anisotropies. The high-energy physics motivated by superstring theory or M-theory generically yields parity violating terms, which may produce a circularly polarized gravitational wave background (GWB) during inflation. In contrast to the standard prediction of inflation with un-polarized GWB, circularly polarized GWB generates non-vanishing TB and EB-mode power spectra of CMB anisotropies. We evaluate the TB and EB-mode power spectra taking into account the secondary anisotropies induced by the reionization and investigate the dependence of cosmological parameters. We then discuss current constraints on the circularly polarized GWB from large angular scales ($\ell \leq 16$) of the three year WMAP data. Prospects for future CMB experiments are also investigated based on a Monte Carlo analysis of parameter estimation, showing that the circular polarization degree, ε, which is the asymmetry of the tensor power spectra between right- and left-handed modes normalized by the total amplitude, can be measured down to $|\varepsilon| \gtrsim 0.35(r/0.05)^{-0.6}$.

1. Introduction

The gravitational wave background (GWB) originating from inflation provides a direct probe of inflation against which we can test inflationary models. In particular, the energy scale of inflation can be estimated from the amplitude of the GWB. Combining with observations of scalar-type fluctuations, the detection of the GWB directly constrains the inflaton potential [1]. Currently, there is no rigorous constraint on the amplitude of the GWB characterized by the tensor-to-scalar ratio, $r \equiv \Delta^2_{\rm gw}(k_0)/\Delta^2_{\mathcal{R}}(k_0)$‡. In the standard scenario of slow-roll inflation, the GWB is expected to have a nearly scale-invariant spectrum, suggesting that the GWB would be detectable in a wide range of wavelengths or frequencies. For a large-scale experiment, polarization anisotropies of the cosmic microwave background (CMB) would be a powerful tool to search for primordial tensor fluctuations. Indeed, post-Planck experiments such as SPIDER§ and CMBpol (or Inflation Probe) in the Beyond Einstein program of NASA‖ is dedicated to measuring the B-mode polarization anisotropies originating from the inflationary GWB, with expected precision level $r \sim 10^{-3}$ [2, 3]. On the other hand, a direct measurement of the stochastic GWB might be possible for a small-scale experiment, especially using space-based laser interferometers [4, 5, 6, 7]. Proposed missions such as the Big-Bang Observer (BBO) [8] and the deci-hertz gravitational-wave observatory (DECIGO) [9, 10] indeed aim at detecting the primordial gravitational waves at the frequencies $f \sim 0.1-1$Hz. Notice that the observational frequencies (or wavelengths) of the space interferometers are greatly different from those of the CMB experiments by 16 orders of magnitude. This implies that the combination of both experiments provides a stringent constraint on the dynamics of inflation.

Meanwhile, motivated by high-energy physics, there are numerous discussions on the corrections to the prediction of standard inflationary models. For example, some inflationary models contain parity-violating interaction terms, as generic predictions of superstring theory/ M-theory [11, 12]. Among these, the Chern-Simons term, which is a higher-order curvature term coupled to the scalar field, appears through the Green-Schwarz mechanism and the cosmological implications of the Chern-Simons terms has been extensively discussed [13, 14, 15, 16, 17, 18, 19, 20]. Such parity-violating terms directly affect the tensor-type perturbations [21, 22] and the polarization modes of the resulting tensor fluctuations becomes asymmetric, leading to a circularly polarized GWB [13, 14, 15, 20]. In this respect, the detection of a circularly polarized GWB would be a direct signature of the cosmological parity-violation and it might also imply that there is a fundamental theory of particle physics beyond the standard model ¶. Since the sensitivity of the forthcoming CMB experiments will be improved significantly, it is timely to explore the possibilities of measuring the signature of new interaction terms through the CMB anisotropies.

---

‡ In this paper, we adopt the conventional value $k_0 = 0.002{\rm Mpc}^{-1}$ as the pivot scale.

§ `http://www.astro.caltech.edu/~lgg/spider_front.htm`

‖ `http://universe.nasa.gov/program/inflation.html`

¶ There exists another source to generate a circular polarized GWB in the early universe, i.e., primordial helical turbulence produced during a first-order phase transition [23, 24]. However, the wavelength of the produced GWB is much smaller than the scale of CMB observations.

In this paper, we discuss in some detail, the observational possibilities of using CMB anisotropy measurements to probe the additional signature imprinted in the primordial gravitational waves. According to [13], a circularly polarized GWB produces a non-trivial correlation between the temperature and the polarization anisotropies. As a result, the cross power spectra between temperature and B-mode polarization becomes non-vanishing. They calculated the TB-mode spectrum in an idealistic situation with a large tensor-to-scalar ratio, neglecting the secondary anisotropies. In the present paper, extending their analysis, we quantitatively evaluate the TB mode spectrum taking into account the effect of secondary anisotropies. Also, we calculate another non-vanishing spectrum, the EB-mode spectrum. Based on the three year data of Wilkinson Microwave Anisotropy Probe (WMAP) [25, 26], we discuss the current constraint on the degree of polarization of the primordial GWB. Further, we address future prospects for the PLANCK satellite or cosmic-variance limited experiments and estimate the extent to which the degree of polarization is constrained from future observations.

This paper is organized as follows. In §2, we briefly describe a mechanism to generate circular polarization of the GWB through the gravitational Chern-Simons term. In §3, the influence of the polarized GWB on the CMB anisotropies is discussed. Based on this, the CMB power spectra originating from circularly polarized GWB are calculated in §4. The current constraints and future prospects are discussed in §5. Finally, §6 is devoted to discussion and conclusions.

2. Polarized gravitational waves from gravitational Chern-Simons term

In this section, we briefly review a mechanism to generate a circularly polarized GWB by the gravitational Chern-Simons (gCS) term [13]. In superstring theory/M-theory, there exist scalar fields coupled with anti-symmetric tensor $F \wedge F \equiv \epsilon^{\alpha\beta\gamma\delta} F_{\alpha\beta} F_{\gamma\delta}$ and/or $R \wedge R \equiv \epsilon^{\alpha\beta\gamma\delta} R_{\alpha\beta}{}^{\mu\nu} R_{\gamma\delta\mu\nu}$, where $F_{\mu\nu}$ is the field strength of the electromagnetic field, $R_{\alpha\beta\gamma\delta}$ is the Riemann tensor, and $\epsilon^{\alpha\beta\gamma\delta}$ is a totally antisymmetric Levi-Civita tensor density [11, 12]. These two terms are referred to as the electromagnetic and the gravitational Chern-Simons term, respectively. The presence of such parity-violating terms plays an important role for several cosmological issues such as structure formation involving axions [14] and leptogenesis or baryogenesis in the early universe [16, 17, 18, 19]. In a homogeneous and isotropic background spacetime, the electromagnetic Chern-Simons term affects neither the evolution of the background spacetime nor the evolution of fluctuations as long as only linear perturbation is considered [27]. Therefore, we consider the gCS term only:

$$S_{CS} = \frac{m_{\rm pl}^2}{64\pi} \int d^4x f(\phi) R \wedge R \ , \tag{1}$$

where $m_{\rm pl}$ is the Planck mass, and the function $f(\phi)$ represents a generic coupling to the scalar field ϕ. In some cases, the scalar field ϕ is identified with the inflaton field during inflation. As long as the inflaton field ϕ is homogeneous and constant in time, equation (1) is just a surface term, and it does not contribute at all to classical gravitational dynamics. Thus, after the end of inflation, we expect that the classical evolution without gCS term is recovered and no anomalous parity violation appears. Moreover, the gCS term also does not affect the evolution of the background and scalar perturbations in the linear regime [21, 22]. Thus, if we ignore the vector perturbation, the influence of the gCS term only appears in the evolution of tensor perturbations.

Let us linearize the Einstein-Hilbert action in the presence of the gCS term. Assuming a flat Friedmann-Robertson-Walker cosmology, the corresponding metric neglecting the scalar perturbation takes the following form:

$$ds^2 = a^2(\eta)[-d\eta^2 + (\delta_{ij} + h_{ij})dx^i dx^j] \ , \tag{2}$$

with h_{ij} being a transverse and traceless tensor, i.e., $\partial^j h_{ij} = h^i{}_i = 0$. Expanding the action up to the second order in the gravitational wave tensor h_{ij}, the evolution equation for tensor fluctuations is obtained in Fourier space as [17]

$$(\mu^s)'' + \left(k^2 - \frac{z^{s\prime\prime}}{z^s}\right)\mu^s = 0 \ , \tag{3}$$

where the subscript $'$ denotes the derivative with respect to η, the amplitude $\mu^s(\eta)$ is defined by $\mu^s(\eta) \equiv z^s h^s$, and the variable z^s is defined by

$$z^s(\eta, \mathbf{k}) \equiv a(\eta)\sqrt{1 - \lambda^s k \frac{f'}{a^2}} \ , \tag{4}$$

$$\begin{cases} \lambda^{\rm R} = +1 \\ \lambda^{\rm L} = -1 \end{cases} , \tag{5}$$

where subscript s stands for a circularly polarized state, s =R, L. We define the right-handed or left-handed circular polarized state by its helicity:

$$h_{ij}(\eta, \mathbf{x}) = \frac{1}{(2\pi)^{3/2}} \int d\mathbf{k} \sum_{s={\rm R,L}} e^s_{ij}(\mathbf{k}) h^s(\mathbf{k}) e^{i\mathbf{k}\cdot\mathbf{x}} \ , \tag{6}$$

$$ik_c \epsilon_a{}^{cd} e^{\rm R}_{bd} = k e^{\rm R}_{ab} \ , \tag{7}$$

$$ik_c \epsilon_a{}^{cd} e^{\rm L}_{bd} = -k e^{\rm L}_{ab} \ , \tag{8}$$

where $e^{\rm R,L}_{ij}$ is the polarization tensor for right-handed or left-handed circular polarization state.

In equation (3), the important point is that the term $z^{s\prime\prime}/z^s$ depends not only on time, but also on the polarization mode. This readily implies that asymmetry of the amplitude in left- and right-handed modes may be produced, leading to a circularly polarized GWB. Apart from the helicity-dependent nature, the evolution equation (3) is a standard form of the harmonic oscillator and one may address the quantum-mechanical generation of the GWB as in the case of simple inflation models. However, there exists a subtle issue on the break-down of linear theory arising from the singularity of the effective potential. Although the analysis under tractable conditions shows that the produced polarization-degree of the primordial fluctuations will be small [17], the result might not be appropriate for the practical cases. The quantitative prediction of the primordial spectrum may be a serious problem in the predictability of the inflation model. We do not discuss in details the primordial spectrum of circular polarized GWBs, but rather, we focus on the detectability of primordial circularly polarized GWBs.

3. CMB power spectra from circular polarization of the GWB

In this section, we discuss CMB anisotropies originated from a circular-polarized GWB. While we particularly consider the circularly polarized GWB, the linearly polarized GWB is shown to have no effect on the CMB power spectra due to the symmetry associated with spin nature of linearly polarized gravitational waves. The details are discussed in Appendix B.

Similar to scalar-type fluctuations, tensor-type fluctuations (i.e., GWB) cause a small perturbation in the photon path, producing CMB temperature and polarization anisotropies [28, 29, 30]. For a temperature fluctuation map $T(\hat{n})$ as a function of sky position $\hat{n}$, let us expand it in the spherical harmonics, $Y_{\ell m}(\hat{n})$. We denote the expansion coefficients by $a^{\rm T}_{\ell m}$. Furthermore, polarization maps for the Stokes parameters $Q(\hat{n})$ and $U(\hat{n})$, which characterize the linear polarization state of the CMB, are obtained and are expanded by the spin-weighted harmonics $Y^{\pm 2}_{\ell m}(\hat{n})$. The coefficients of these polarization anisotropies are decomposed into an electric part, $a^{\rm E}_{\ell m}$, and a magnetic part, $a^{\rm B}_{\ell m}$ [28]. Apart from a tiny non-Gaussianity, these coefficients $a^{\rm X}_{\ell m}$ (X=T,E,B) are statistically characterized by Gaussian statistics with zero mean. In the case of the two-point statistics of CMB temperature and polarization anisotropies are completely specified by the six (TT, EE, BB, TE, TB ,EB) power spectra defined as the rotationally-invariant quantities:

$$C_\ell^{\rm XX'} \equiv \frac{1}{2\ell+1}\sum_m \left\langle \frac{(a^{\rm X*}_{\ell m}a^{\rm X'}_{\ell m} + a^{\rm X}_{\ell m}a^{\rm X'*}_{\ell m})}{2} \right\rangle \ , \tag{9}$$

in terms of which,

$$\langle a^{\rm X*}_{\ell' m'} a^{\rm X'}_{\ell m}\rangle = C_\ell^{\rm XX'}\delta_{\ell\ell'}\delta_{mm'} \ , \tag{10}$$

where X and X$'$ stand for T,E and B.

Usually, the tensor perturbation produces both EE- and BB-mode polarization power spectra, but cross power spectra of TB- and EB-modes should vanish because of the parity conservation of the perturbations. However, a circularly-polarized GWB manifestly violates the parity symmetry, leading to non-zero values of the TB- and EB-mode power spectra. To be more precise, we write down the relation between the CMB anisotropy power spectra and the primordial power spectra of the GWB [28]:

$$C_\ell^{{\rm XX'}(t)} = (4\pi)^2 \int k^2 dk [P^{t{\rm L}}(k) + P^{t{\rm R}}(k)]\Delta^t_{{\rm X}\ell}(k)\Delta^t_{{\rm X'}\ell}(k) \ ; \tag{11}$$

for XX$'$=TT, EE, BB and TE, and

$$C_\ell^{{\rm YY'}(t)} = (4\pi)^2 \int k^2 dk [P^{t{\rm L}}(k) - P^{t{\rm R}}(k)]\Delta^t_{{\rm Y}\ell}(k)\Delta^t_{{\rm Y'}\ell}(k) \ ; \tag{12}$$

for YY$'$=TB and EB. Here, subscript $^{(t)}$ indicates the contribution from tensor mode and $\Delta^t_{\mathrm{X}\ell}(k)$ is photon's transfer function for X (see Appendix A). The quantities $P^{t\,\mathrm{s}}(k)$ ($s = \mathrm{L}$, R) are the primordial power spectra of GWB in terms of the circular polarization basis. The circularly polarized GWB implies $P^{t\mathrm{L}}(k) \neq P^{t\mathrm{R}}(k)$, which clearly yields non-zero TB- and EB-mode power spectra.

Here, to characterize the polarization degree of GWB, we introduce the new variable ε defined by

$$P^{t\mathrm{R}}(k) \equiv \frac{1}{2}\,(1+\varepsilon)\,P^t(k)\ , \tag{13}$$

$$P^{t\mathrm{L}}(k) \equiv \frac{1}{2}\,(1-\varepsilon)\,P^t(k)\ , \tag{14}$$

$$P^t(k)\ \ \equiv P^{t\mathrm{L}}(k) + P^{t\mathrm{R}}(k)\ . \tag{15}$$

The variable $(\varepsilon+1)/2$ is the fractional power of right-handed GWB with respect to that of total GWB. Therefore ε characterizes the degree of parity violation. For instance, $\varepsilon = -1$, 0 and 1 respectively indicate perfectly left-handed polarized, un-polarized, and perfectly right-handed polarized GWB. Hereafter, we simply assume that ε is scale-independent, which might be a good approximation in the slow-roll regime [17].

Notice that the TT-, EE-, BB- and TE-mode power spectra remain unchanged irrespective of the parity violation. Thus, for CMB experiments, a measurement of the TB- and EB-mode power spectra is a unique probe to search for the parity violation in the early universe. Observationally, TB and EB-mode spectra are often used for a consistency null check to determine whether or not the foreground contamination is removed [26]. However, in our case, the non-vanishing values of the TB and EB-modes are essential. In this sense, detection of a circularly polarized GWB should be carefully investigated in practice, since the incomplete foreground subtraction may lead to a false detection. Nevertheless, in the next section, we will show that TB- and EB-mode power spectra originating from the circularly polarized GWB have some characteristic features, especially on large-angular scales, which might be helpful to discriminate the primordial origin from foreground contamination. Moreover, note that the signals of TB- and EB-modes power spectra originating circularly polarized GWB do not depend on the wavelength of CMB photon in contrast to some foreground sources.

Finally, we comment on the TB- and EB-mode power spectra generated through the electromagnetic Chern-Simons term, $g(\chi)F\wedge F$. When the scalar field χ is identified with the ghost or the quintessence field, this term affects the CMB polarizations after photon decoupling, through the rotation of the photon's polarization axis. As a result, we obtain non-vanishing TB- and EB-modes like $C_\ell^{\mathrm{TB}} = C_\ell^{\mathrm{TE}}\sin 2\alpha$, where α is the rotation angle of the polarization axis [13, 31, 32, 33]. This is even true in the absence of tensor fluctuations, since a non-vanishing contribution is still obtained from scalar type fluctuations. Thus, for a small tensor-to-scalar ratio, the shape of TB-mode power spectrum is essentially the same as that of the scalar-type TE-mode spectrum. In this respect, a non-vanishing TB-mode spectrum by the electromagnetic Chern-Simons term may be clearly distinguished from that produced from circularly polarized GWBs.

Note that the non-vanishing TB-mode is also obtained by the Faraday rotation through intervening magnetic fields [34]. The Faraday rotation depends on the CMB photon frequency [35] and it also alters the angular dependence of the TB-mode power spectrum. In this paper, we do not consider these two effects and just focus on the CMB power spectra from the circular polarized GWB.

4. TB- and EB-mode power spectra from a circularly polarized GWB

We now consider the amplitude and the shape of the TB- and EB-mode power spectra discussed in §3, taking into account the secondary anisotropies. We will show that the effect of reionization greatly enhances the amplitude of the TB-mode at large angular scales. On the other hand, the effect of weak lensing is shown to be negligibly small. In this and following sections, we adopt the following cosmological parameters as fiducial model parameters, which are taken from the best-fit values of the three year WMAP data (ΛCDM+tensor), except for the tensor-to-scalar ratio $r = 0.1$:

$$\begin{aligned} &\Omega_{\rm b}h^2 = 0.0233,\ \Omega_{\rm CDM}h^2 = 0.0962,\ \Omega_{\rm K} = 0,\ h = 0.787, \\ &\tau_{\rm ri} = 0.09,\ \Delta^2_{\mathcal{R}}(0.002/{\rm Mpc}) = 2.1 \times 10^{-9}\ , n_{\rm S} = 0.984,\ r = 0.1. \end{aligned} \tag{16}$$

For simplicity, we assume the slow-roll consistency relation, $n_{\rm T} = -r/8$, and the vanishing running spectral index. The power spectra of CMB anisotropies presented here are all calculated based on the CAMB code [38], with suitable modification to compute TB- and EB-mode spectra.

4.1. Primary anisotropies

Let us first show the primary anisotropies of the TB- and EB-mode power spectra originating from the circularly polarized GWB of a primordial origin.

In Figure 1, specifically setting the parameter $\varepsilon = 1$ corresponding to the right-handed polarized GWB, the TB- and EB-mode power spectra are plotted under the fiducial cosmological model except for the re-ionization parameter, $\tau_{\rm ri} = 0$. The results are then compared with the TT- and BB-mode spectra for the tensor fluctuations[+].

Similarly to the BB-mode power spectrum, the TB- and EB-mode spectra have a peak at $\ell \sim \ell_R$, corresponding to the horizon scale at recombination (for details of the location of the BB-mode peak, see [36]). Also, at higher multipoles with $\ell > 200$, oscillatory behavior appears, which simply reflects the oscillations of the gravitational waves after the horizon re-entry time during the recombination epoch. A closer look at cross spectra reveals that while the EB-mode spectrum has many crossing points at higher multipoles, the TB-mode spectrum has one crossing point and the sign of the spectra is only changed around $\ell \sim 70$. Further, the amplitude of the EB-mode spectrum is extremely small compared to the one naively expected from the BB-(EE-)mode tensor

[+] Note that the sign of the TB-mode power spectrum plotted here is opposite to the one in Ref.[13]. Perhaps, this differences come from the definition of polarization bases, $e_{ab}^{\rm R,L}$. Our definition follows that of Ref.[17], i.e., equations (7) and (8).

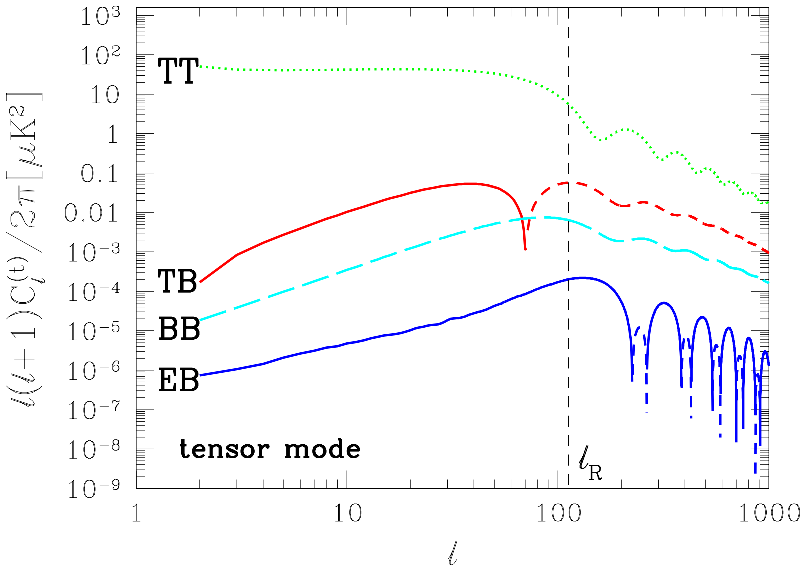

Figure 1. The temperature and polarization cross spectra, $C_\ell^{\mathrm{TB}(t)}$ and $C_\ell^{\mathrm{EB}(t)}$, from circularly polarized gravitational waves. Here, setting the reionization optical depth, $\tau_{\mathrm{ri}} = 0$, the absolute values of the cross power spectra are plotted for fiducial model with $\varepsilon = +1$. In these plots, the negative correlation is indicated by the short-dashed lines. As a reference, TT (*dotted*) and BB-mode (*long-dashed*) power spectra are also plotted. The vertical line labeled by $\ell_R(\sim 100)$, roughly corresponds to the angular size of the horizon radius at recombination epoch.

spectrum. These characteristic behaviors basically come from the projection factors in the photon's transfer function $\Delta^t_{\mathrm{X}\ell}(k)$ (X=T, E, B). In Appendix C, the reasons for these properties are discussed in some detail.

Apart from a tiny dependence on the density parameters such as Ω_{b} and Ω_Λ (e.g., see Ref.[37] in the case of the BB-mode spectrum), the amplitude of primary TB- and EB-mode spectra are mainly determined by the tensor-to-scalar ratio r and the fractional power of circular polarization ε. In Figures 2 and 3, the dependence of the TB- and BE-mode spectra on ε and r (or n_{T}) are shown respectively. Both of the parameters ε and r linearly alter the amplitude of spectra, but the degree of circular polarization, ε, allows us to change the over-all sign. This is the key to discriminate the polarization states of the GWB. Note that in plotting Figure 3, we strictly keep the slow-roll consistency relation, $n_T = -r/8$. However, the change of the spectral shape is very small and it would be difficult to observe it.

4.2. Effects of secondary anisotropies

Let us move to the discussion on the effects of secondary anisotropies generated after the recombination epoch.

There are two possible sources to produce a large-angular scale anisotropy: reionization and the weak lensing. Among these, the weak lensing effect represents the

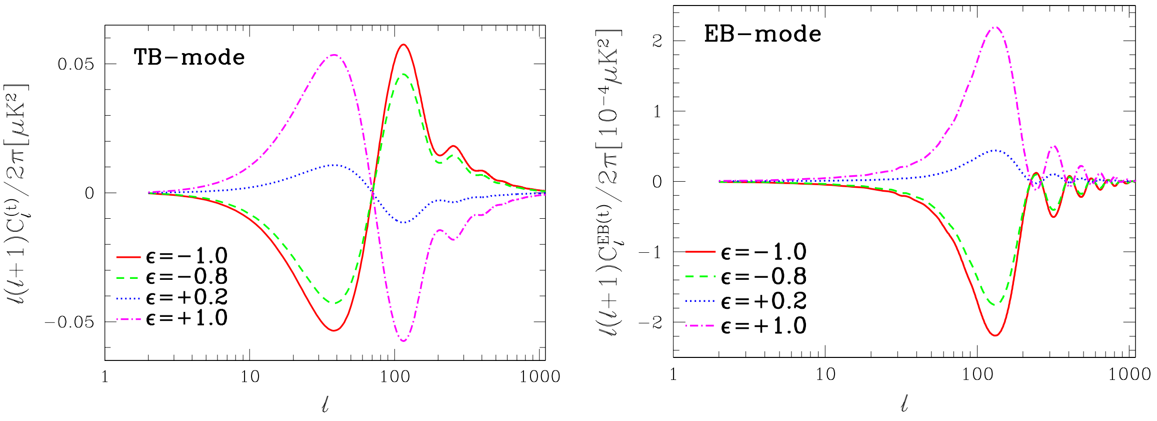

Figure 2. Dependence of circular polarization degree, ε, on the TB- (*left*) and EB-mode (*right*) power spectra for the fiducial model except for the reionization optical depth, $\tau_{\rm ri} = 0$.

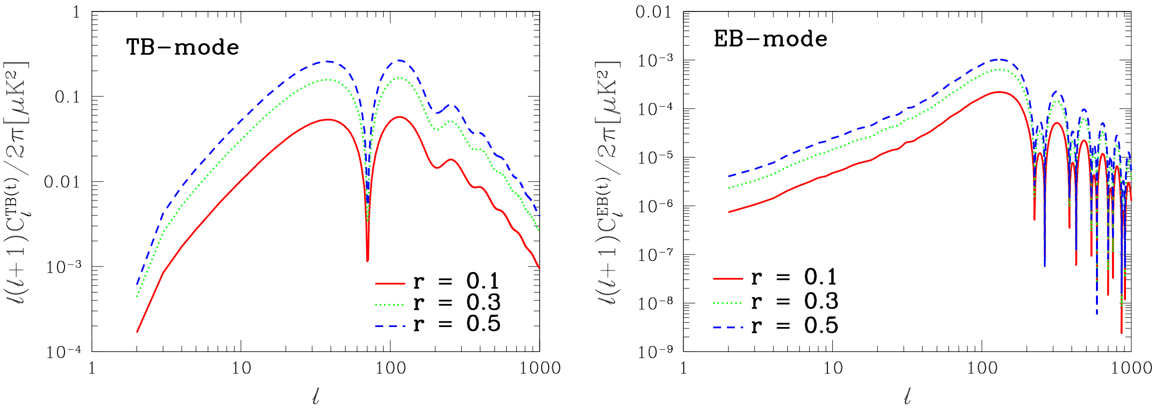

Figure 3. Dependence of the tensor-to-scalar ratio, r, on the TB- (*left*) and EB-mode (*right*) power spectra for the fiducial model with $\varepsilon = -1.0$. In these plots, the reionization optical depth is set to $\tau_{\rm ri} = 0$, keeping the slow-roll consistency relation $n_{\rm T} = -r/8$.

gravitational deflection of a photon's propagation direction by the large-scale structure and it distorts the temperature and polarization maps of the CMB (see [42] for a review). In particular, the effects from weak lensing are known as the big obstacle to detect the gravitational waves from the BB-mode power spectrum, since weak lensing newly creates the B-mode polarization anisotropy from the scalar-type perturbations, which would dominate over the tensor fluctuation at $\ell \gtrsim 100$. In the case of temperature-polarization cross spectra, however, transformation properties of E- and B-modes do not allow the production of a new TB-mode correlation from the scalar-type perturbations. This is also true for the EB-mode spectrum. As a result, the lensing effects on the TB- and EB-mode spectra are negligibly small. Detailed discussion on the effects of weak lensing are presented in Appendix D.

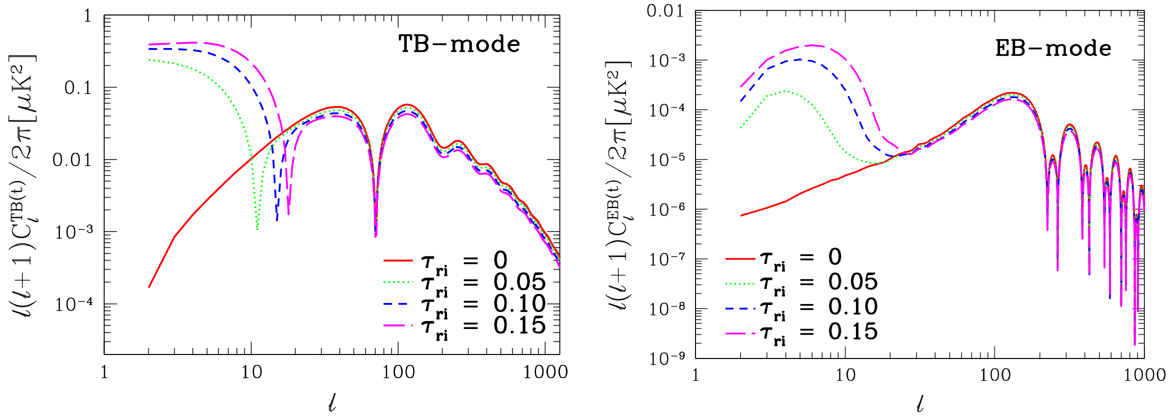

Figure 4. Dependence of the reionization optical depth, $\tau_{\rm ri}$ on the TB- (*left*) and EB-mode (*right*) power spectra for the fiducial model with $\varepsilon = -1.0$. A large enhancement of the amplitude arises due to the re-scattering of the CMB photons during reionization.

On the other hand, the reionization of the universe drastically changes the large-scale anisotropies. Although details of the reionization history are model-dependent and are currently uncertain, its effect on the CMB power spectra is mainly characterized by the optical depth to the beginning of reionization, $\tau_{\rm ri}$ [40, 41]. In Figure 4, we show the TB- and EB-mode power spectra for various values of the reionization optical depth. Similar to the polarization spectra of scalar-type perturbations, the resultant power spectra are greatly amplified and a larger value of $\tau_{\rm ri}$ leads to a large amplitude of TB- and BE-mode at lower multipoles. This is essentially the same reason as in the scalar TE- and EE-mode spectra that the polarization anisotropies of the CMB photon are newly created from a primary anisotropy by Thomson scattering at reionization. The power spectra are sharply peaked at large-angular scales and the peak position $\ell_{\rm ri}$ is roughly estimated as $\ell_{\rm ri} \sim \sqrt{z_{\rm ri}}$ [41]. One interesting observation is that a new zero-crossing point appears around $\ell \sim 10-20$ in the TB-mode spectrum and the amplitude of lower multipoles $\ell < 6$ eventually changes its sign.

Although the precise form of the spectrum is difficult to predict analytically, the peak height of the spectrum caused by the reionization is roughly estimated as follows. First of all, the reionization reduces the fraction of photons reaching us from the recombination epoch. This is basically proportional to $\exp(-\tau_{\rm ri})$. Further, in the simple approximation with instantaneous reionization, the visibility function $g(\eta) = \tau' \, e^{-\tau}$ in equation (A.5) has a sharp peak around the reionization redshift $z_{\rm ri}$, in addition to the primary peak around the recombination epoch. These effects explicitly appear in the photon transfer function $\Delta^t_{{\rm X}\ell}$ or $\widetilde{\Delta}^t_{\rm X}$. Keeping this point in mind, from equation (A.10), the transfer function for temperature fluctuation becomes

$$\widetilde{\Delta}^t_{\rm T}(k,\mu) \simeq -\int_0^{\eta_0} d\eta \, e^{i\,\mu\,k\,(\eta-\eta_0)}\, h' e^{-\tau} \approx e^{-\tau_{\rm ri}} \widetilde{\Delta}^{t{\rm NR}}_{\rm T} \,, \tag{17}$$

where we have only considered the dominant term. Here, $\widetilde{\Delta}^{t{\rm NR}}$ represents the transfer function in the absence of reionization. In a similar manner, the transfer function for polarization fluctuations $\widetilde{\Delta}^t_{\rm P}$, given by (A.13), is approximately described by

$$\widetilde{\Delta}^t_{\rm P}(\eta_0,k,\mu)=\int_0^{\eta_0}d\eta\, e^{i\,\mu\,k\,(\eta-\eta_0)}(-g\,\Psi)\approx\frac{1}{10}[1-e^{-\tau_{\rm ri}}]\,\widetilde{\Delta}^{t{\rm NR}}_{\rm T}\ . \tag{18}$$

Here, the source function Ψ has been roughly evaluated from the monopole component of the temperature fluctuation as $\Psi\simeq(1/10)\,\widetilde{\Delta}^t_{\rm T0}$. The prefactor, $[1-e^{-\tau_{ri}}]$, indicates the fractional probability of photons scattered after the reionization before reaching the observer, leading to a new polarization anisotropy.

Based on the above approximations, the peak height of the power spectra is roughly estimated around $\ell\sim 2$. From equations (A.1)–(A.9), we obtain

$$C^{{\rm TT}(t)}_{\ell\sim2}\ \approx e^{-2\tau_{\rm ri}}\,C^{{\rm TT}(t){\rm NR}}_{\ell\sim2}\ , \tag{19}$$

$$C^{{\rm EE}(t)}_{\ell\sim2}\ \approx\frac{1}{100}[1-e^{-\tau_{\rm ri}}]^2\,C^{{\rm TT}(t){\rm NR}}_{\ell\sim2}\ , \tag{20}$$

$$C^{{\rm BB}(t)}_{\ell\sim2}\ \approx\frac{1}{100}[1-e^{-\tau_{\rm ri}}]^2\,C^{{\rm TT}(t){\rm NR}}_{\ell\sim2}\ , \tag{21}$$

$$\left|C^{{\rm TB}(t)}_{\ell\sim2}\right|\ \approx\frac{|\varepsilon|}{10}e^{-\tau_{\rm ri}}[1-e^{-\tau_{\rm ri}}]\,C^{{\rm TT}(t){\rm NR}}_{\ell\sim2}\ , \tag{22}$$

where $C^{{\rm TT}(t){\rm NR}}_{\ell}$ stands for the temperature power spectrum for tensor mode without reionization. For fiducial cosmological parameters, the amplitude of the TB-mode at $\ell\sim2$ is evaluated as

$$\left|C^{{\rm TB}(t)}_{\ell\sim2}\right|\approx 4\,\times\,10^{-1}\ |\varepsilon|\left(\frac{r}{0.1}\right)\ [\mu{\rm K}^2]\ . \tag{23}$$

With an appropriate range of the reionization optical depth $0.05\lesssim\tau_{\rm ri}\lesssim0.15$, the approximations (19)–(22) agree reasonably with numerical results of the power spectra.

As a summary of this section, we present the full CMB power spectra, i.e., the combined results of the contributions from both the scalar- and tensor-type perturbations. Figure 5 shows the results, specifically choosing the degree of polarization as $\varepsilon=0.1$. With a slightly large value of the tensor-to-scalar ratio $r=0.1$, the amplitude of the TB-mode spectrum becomes comparable to the EE-mode spectrum. Interestingly, the amplitude of the TB-mode spectrum also exceeds the BB-mode amplitude at large angular scales. This is even true for small degree of polarization, $\varepsilon\gtrsim0.01$.

5. Observational constraints on the circular polarization of the GWB

Having understood the basic properties of the TB- and EB-mode power spectra, we now proceed to discuss the observational aspects for detecting a circularly polarized GWB. In section 5.1, for illustrative purposes, constraint on the degree of polarization of the GWB is derived based on the three year WMAP data. In practice, we must wait for future polarization experiments in order to get a meaningful constraint. In section 5.2, future prospects for measuring the degree of polarization of the GWB are addressed based on a Monte Carlo analysis of parameter estimation.

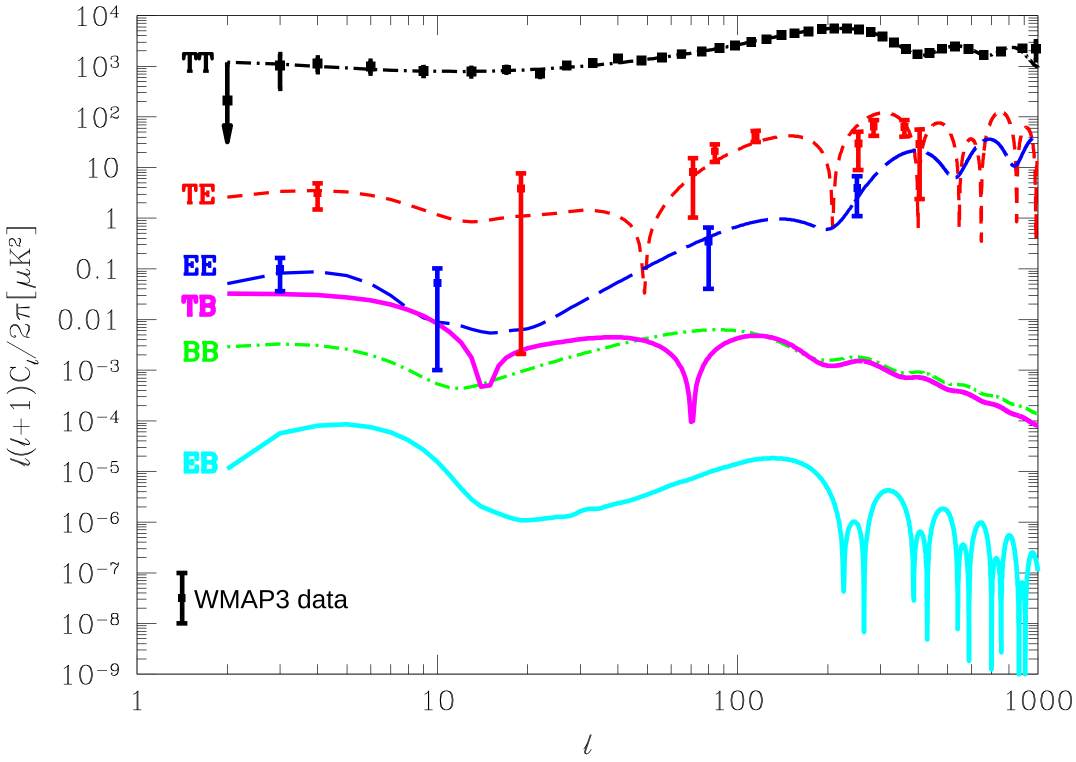

Figure 5. CMB power spectra for the fiducial cosmology with $\varepsilon = +0.1$, including both scalar and tensor mode. For comparison, three year WMAP data of TT, TE and EE-mode power spectra are plotted. At large-angular scale, the amplitude of the TB-mode (*magenta, solid*) exceeds the BB-mode power spectrum (*green, dot-short dashed*) and becomes comparable to the EE-mode power spectrum(*blue, long-dashed*).

5.1. Constraints from three year WMAP data

Previous sections reveal that the effect of reionization largely amplifies the lower-multipole anisotropies and the amplitude of the TB-mode spectrum at multipoles $\ell \sim 2 - 10$ would be a clear indicator to measure the polarization states of the GWB. While currently no definite detection of the tensor-type fluctuations has been reported, it is a good exercise to consider how one can constrain the circularly polarized GWB from lower-multipole data. For this purpose, we use the TB- and EB-mode power spectra taken from the three year WMAP data, currently the highest precision data at large-angular scales [26]. Here, particularly using the lower-multipole data of $\ell \leq 16$, we perform a global parameter estimation together with the TT-, EE- and TE-mode data. We use the publicly available Markov-Chain Monte Carlo code, COSMOMC [45], which we modified to compute the TB- and EB-mode power spectra originating from a circularly polarized GWB.

In the present analysis, we use the likelihood function for TT-, EE- and TE-mode spectra available on the LAMBDA website [*]. As for the TB- and EB-mode data, we simply assume the Gaussian likelihood function:

$$\mathcal{L}_{\rm TB/EB} = \exp\left(-\frac{\chi^2_{\rm TB/EB}}{2}\right) , \tag{24}$$

with

$$\chi^2_{\rm TB/EB} = \sum_\ell \frac{(\overline{C}_\ell^{\rm TB/EB} - \widehat{C}_\ell^{\rm TB/EB})^2}{\sigma_\ell^2} , \tag{25}$$

where the quantities $\overline{C}^{\rm TB/EB}$ and $\widehat{C}^{\rm TB/EB}$ respectively denote the theoretical value and the experimental data of the TB- or EB-mode power spectra. The quantity σ_ℓ^2 denotes the variance of estimated power spectra at each multipole, corresponding to the diagonal component of the covariance matrix. Strictly speaking, the assumption (24) is not valid for the three year WMAP data. For full-sky coverage, the exact likelihood function significantly deviates from the Gaussian likelihood function at lower multipoles [46]. Nevertheless, just for illustrative purpose, we adopt the Gaussian form (24), since we do not know the precise form of likelihood function suitable for WMAP experiment including TB- and EB-mode power spectra. A more rigorous treatment including the non-Gaussianity in the likelihood function will be discussed in the next subsection.

To derive the constraint, we consider a spatially flat cosmology and treat the following eight parameters as free parameters:

$$(\Omega_{\rm b}h^2,\ \Omega_{\rm CDM}h^2,\ \theta,\ \tau_{\rm ri},\ n_{\rm S},\ A_{\rm S},\ r,\ \varepsilon) \tag{26}$$

where θ is the ratio of the sound-horizon scale to the angular diameter distance. The parameters $n_{\rm S}$ and $A_{\rm S}$ are the scalar spectral index and the amplitude of the curvature perturbation, respectively. Then, keeping the slow-roll consistency relation, $n_T = -r/8$, we perform a global estimation of the cosmological parameters.

Figure 6 shows the constraints on the tensor-to-scalar ratio r and the circular polarization degree ε by marginalizing over the other cosmological parameters. Top panel plots the projected two-dimensional contours of 68% (blue) and 95% (light-blue) confidence regions, while bottom panels give the marginalized one-dimensional posterior distribution for the parameters ε (*left*) and r (*right*). Note that the constraints on the other cosmological parameters are also derived and our constraints reasonably match those obtained by the WMAP team.

From Figure 6, no definite constraint on the degree of circular polarization was obtained. This is simply because the uncertainty in the tensor-to-scalar ratio r is still large. Although the 95% confidence limit of r is slightly reduced to $r < 0.59$ compared to the WMAP result with $r < 0.65$[♯], this is still consistent with the vanishing tensor-to-scalar ratio $r = 0$. A closer look at the posterior distribution reveals that there is a local maximum around $\varepsilon \sim -1$. However, observational errors of the TB- and EB-mode

---

[*] `http://lambda.gsfc.nasa.gov/product/map/dr2/likelihood_get.cfm`

[♯] This result is obtained using the three year WMAP data with TT-, TE- and EE-mode. Note that the tightest constraint is $r < 0.30$ with WMAP3+SDSS.

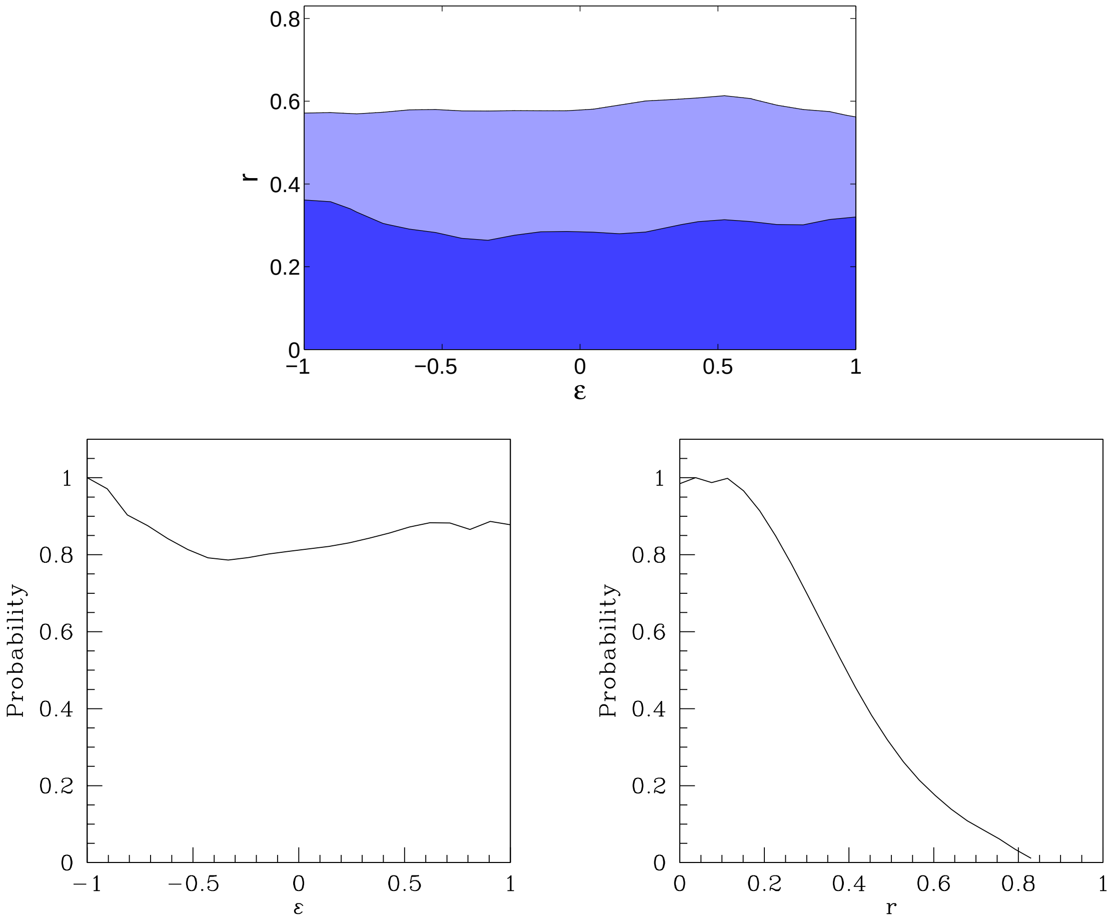

Figure 6. Constraints on the circularly polarized GWB from the three year WMAP data. Top panel shows the 68% (*blue*) and the 95% (*light-blue*) confidence regions of the parameters r and ε. The results are obtained by marginalizing over the other cosmological parameters. Bottom panel shows the posterior distribution for the degree of polarization ε (*left*) and the tensor-to-scalar ratio r (*right*).

spectra are very large and the agreement between theory and observation is not visually clear. Therefore, the significance of non-vanishing ε is very low. We conclude that no meaningful constraint on the degree of circular polarization is obtained.

5.2. Future prospects

Focusing on the prospects for measuring the circular polarization degree, we estimate the expected constraints derived from the future experiments. In what follows, assuming the complete subtraction of the foreground sources, we address principal aspects for detecting a circularly polarized GWB. We examine the two specific cases: forthcoming experiment by PLANCK satellite and a cosmic-variance limited experiment idealistically corresponding to the next-generation CMB measurement.

As mentioned in the previous subsection, the Gaussian likelihood function for the

C_ℓ's is an inadequate assumption at lower multipoles [46] and the non-Gaussianity arising from the cosmic variance should be properly taken into account. Further, notice the large cosmic variance for the TB-mode power spectrum. This is deduced from the diagonal component of the covariance matrix, $\mathrm{Cov}_\ell^{\mathrm{TB}}$:

$$\mathrm{Cov}_\ell^{\mathrm{TB}} = \frac{(\overline{C}_\ell^{\mathrm{TT}} + N_\ell^{\mathrm{TT}})(\overline{C}_\ell^{\mathrm{BB}} + N_\ell^{\mathrm{BB}}) + (\overline{C}_\ell^{\mathrm{TB}})^2}{(2\ell+1) f_{\mathrm{sky}}} \ , \tag{27}$$

which roughly corresponds to the estimation error of the power spectrum. Here, N_ℓ^{TT} and N_ℓ^{BB} denote the experimental noises for temperature and polarization maps, and f_{sky} is the fractional sky coverage. In the above expression, theoretical power spectrum $\overline{C}_\ell^{\mathrm{TT}}$ includes the contribution from both the scalar- and tensor-type perturbations. Thus, for a small tensor-to-scalar ratio, the dominant contribution to $\mathrm{Cov}_\ell^{\mathrm{TB}}$ always comes from the first term $(\overline{C}_\ell^{\mathrm{TT}} + N_\ell^{\mathrm{TT}})(\overline{C}_\ell^{\mathrm{BB}} + N_\ell^{\mathrm{BB}}) \simeq \overline{C}_\ell^{\mathrm{TT}}\overline{C}_\ell^{\mathrm{BB}}$, leading to a large uncertainty in the power spectrum estimation. This is true even in the absence of the primary TB-mode anisotropy. In this respect, definite detection of the degree of circular polarization requires a larger value of ε and a proper treatment of the cosmic-variance is crucial to get the correct constraints.

Keeping the above remarks in mind, we adopt the non-Gaussian likelihood function derived in Appendix E:

$$\begin{aligned} -2\ln\mathcal{L} = \sum_\ell (2\ell+1) f_{\mathrm{sky}} \Bigg\{ \ln\left(\frac{\overline{C}_\ell^{\mathrm{TT}}\overline{C}_\ell^{\mathrm{BB}} - (\overline{C}_\ell^{\mathrm{TB}})^2}{\widehat{C}_\ell^{\mathrm{TT}}\widehat{C}_\ell^{\mathrm{BB}} - (\widehat{C}_\ell^{\mathrm{TB}})^2} \right) \\ + \frac{\widehat{C}_\ell^{\mathrm{TT}}\overline{C}_\ell^{\mathrm{BB}} + \overline{C}_\ell^{\mathrm{TT}}\widehat{C}_\ell^{\mathrm{BB}} - 2\overline{C}_\ell^{\mathrm{TB}}\widehat{C}_\ell^{\mathrm{TB}}}{\overline{C}_\ell^{\mathrm{TT}}\overline{C}_\ell^{\mathrm{BB}} - (\overline{C}_\ell^{\mathrm{TB}})^2} - 2 \Bigg\} \ . \end{aligned} \tag{28}$$

Again, the quantities $\overline{C}_\ell^{\mathrm{XY}}$ and $\widehat{C}_\ell^{\mathrm{XY}}$ respectively denote the theoretical and the estimated values of the power spectra. Note that the likelihood function (28) becomes maximum when $\overline{C}_\ell^{\mathrm{XY}} = \widehat{C}_\ell^{\mathrm{XY}}$. The above expression is the exact result for the experimental data with full-sky coverage $f_{\mathrm{sky}} = 1$, but it still provides a good description for an experiment with almost full-sky coverage, like PLANCK.

Based on the likelihood function (28), we perform a likelihood analysis to estimate the sensitivity of future experiments for constraining the parameters r and ε. To do this, we use the TT-, BB- and TB-mode power spectra with multipoles $\ell \leq 100$. The data points for each power spectrum $\widehat{C}_\ell^{\mathrm{XY}}$ are exactly set to the fiducial theoretical values. This is equivalent to the averaged data set over the infinite number of mock samples [47]. For the cosmic-variance limited experiment, we just use the form (28) and simply set f_{sky} to unity. On the other hand, for the PLANCK setup, both the theoretical and experimental power spectra in the likelihood function (28) are replaced with those including noise bias contributions as $\overline{C}_\ell^{\mathrm{TT/BB}} \to (\overline{C}_\ell^{\mathrm{TT/BB}} + N_\ell^{\mathrm{TT/BB}})$ and $\widehat{C}_\ell^{\mathrm{TT/BB}} \to (\widehat{C}_\ell^{\mathrm{TT/BB}} + N_\ell^{\mathrm{TT/BB}})$. The noise power spectra for the PLANCK experiment are given by

$$N_\ell^{\mathrm{XX}} = \omega_{\mathrm{X}}^{-1} W_\ell^{-2} = (\sigma_{\mathrm{P,X}}\,\theta_{\mathrm{FWHM}})^2 \exp\left[\frac{\ell(\ell+1)}{\ell_{\mathrm{beam}}^2}\right] \tag{29}$$

with subscript XX being $XX = TT$ or BB. The quantity ω_X is the weight factor per solid angle, W_ℓ is the beam window function, and the beam size, $\ell_{\rm beam}$, is given by $\ell_{\rm beam} = \sqrt{8\ln 2}/(\theta_{\rm FWHM})$ for the Gaussian beam. For the average sensitivity per pixel, $\sigma_{P,X}$, and angular resolution, θ_{FWHM}, we adopt the values for the high frequency instruments of 100, 143 and 217GHz channels (see Table 1.1 of [44] for instrumental performance). The sky coverage of PLANCK is assumed to be $f_{\rm sky} = 0.65$, corresponding to a ±20 degrees Galactic cut.

Figure 7 displays the results for the expected sensitivity of future experiments to the constraint on the degree of circular polarization ε for the specific tensor-to-scalar tensor ratio: $r = 0.3$ (*top*), 0.1 (*middle*) and 0.05 (*bottom*). In each panel, the marginalized 68% confidence regions of the posterior distribution for ε are plotted for PLANCK (*red*) and cosmic-variance limited (*yellow*) experiments, as a function of the true input value, $\varepsilon_{\rm true}$ ††. At first sight, a definite detection of the degree of circular polarization seems difficult for small tensor-to-scalar ratios. This is simply due to the large cosmic variance coming from the contribution $\overline{C}_\ell^{\rm TT}\overline{C}_\ell^{\rm BB}$ (see Eqs.(27) and (28)), in which the TT-mode spectrum $\overline{C}_\ell^{\rm TT}$ always gives a large value and is not much affected by the tensor-to-scalar ratio. From Figure 7, the PLANCK experiment hardly constrains the degree of circular polarization at $r \lesssim 0.1$, below which the 68% confidence level extends over the region $\epsilon_{\rm obs} < 0$ and one cannot clearly discriminate between polarized and un-polarized GWBs.

On the other hand, for the idealistic situation of cosmic-variance limited experiment, there still exists a window to distinguish a signature of circularly polarized GWB from the cosmic-variance dominated data. From Figure 7, the detectable level of the polarization degree can be read off:

$$|\varepsilon_{\rm obs}| \gtrsim 0.35 \left(\frac{r}{0.05}\right)^{-0.61} . \tag{30}$$

Note that this estimate is roughly consistent with the one obtained by Ref.[13], in which the authors reported that post-PLANCK experiment might conceivably be able to discriminate a value as small as $\varepsilon \sim 0.08$ for the tensor-to-scalar ratio $r = 0.7$, comparable to our estimate of the detectable level, 0.07. However, they did not properly take into account the effects of reionization. Further, they only used the TB-mode spectrum to derive a minimum detectable ε. In this respect, close agreement between ours and Ref.[13] might be regarded as an accidental one.

Anyway, a realistic value of the tensor-to-scalar ratio is expected to be much smaller than unity. Our results imply that a large value of ε is generally required in order to falsify the possibility of an un-polarized GWB. However, we do not theoretically exclude the possibility of a perfectly polarized GWB. Though difficult, it is still worthwhile to explore a signature of parity violation in the universe with future CMB experiments.

---

†† The upper and lower values of the 68% confidence region, $[\varepsilon_1, \varepsilon_2]$, around the best-fit value are estimated from the marginalized posterior distribution $P(\varepsilon_{\rm obs})$ as $\int_{\varepsilon_1}^{\varepsilon_2} d\varepsilon_{\rm obs} P(\varepsilon_{\rm obs}) = 0.68$ under equi-probability, $P(\varepsilon_1) = P(\varepsilon_2)$. In cases with ε_2 (ε_1) reaching 1 (−1), we simply set it to 1 (−1).

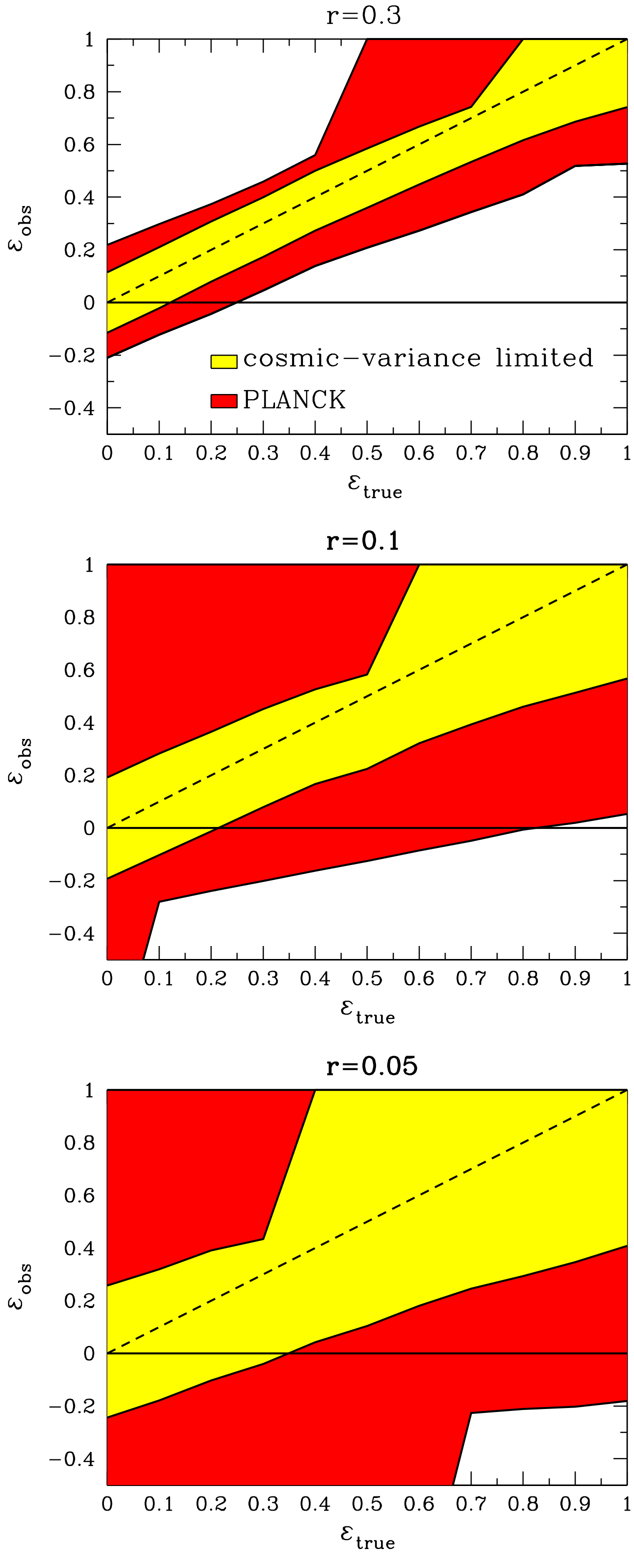

Figure 7. Expected sensitivity of future experiment to the constraint on the circular polarization degree ε for the specific tensor-to-scalar ratio: $r = 0.3$(*top*), $r = 0.1$(*middle*) and $r = 0.05$(*bottom*). In each panel, the one-dimensional marginalized 68% confidence region of the estimated value of circular polarization degree, $\varepsilon_{\rm obs}$, is plotted as a function of the true input value, $\varepsilon_{\rm true}$. The *yellow* and *red* shaded region respectively represents the expected sensitivity of the PLANCK and ideal cosmic-variance limited experiments. The dashed line indicates $\varepsilon_{\rm true} = \varepsilon_{\rm obs}$.

6. Discussion and conclusions

We have extensively discussed the detectability of the polarized states of primordial gravitational waves imprinted in the CMB anisotropies. In the early universe, the parity violation term originating from superstring theory or M-theory generically arises, which may produce a circularly polarized GWB during inflation. Such asymmetrically polarized gravitational waves induce a non-trivial correlation of CMB anisotropies between temperature and polarization modes. We have calculated the power spectra of CMB anisotropies generated from a circularly polarized GWB (i.e., TB- and EB-mode spectra). Taking into account the secondary anisotropies, we found that the effect of reionization creates a large amplitude of the lower multipoles of TB- and EB-mode spectra, which may be helpful to constrain the tensor-to-scalar amplitude ratio, r, as well as the degree of circular polarization of the GWB, ε. We then move to discuss observational aspects for detecting a circular polarized GWB. Using the three year WMAP data, we demonstrated how one can constrain the parameters ε and r from TB- and EB-mode data. For future prospects, we derive an expected sensitivity of representative experiments, i.e., PLANCK and cosmic-variance limited experiments, to the degree of the circular polarization. While the PLANCK experiment seems difficult to answer whether the GWB is polarized or not, post PLANCK experiments dominated by the cosmic-variance may give a meaningful constraint on the parity violation in the early universe. This result is interesting in the sense that the next-generation laser interferometers will also be sensitive to the circular polarization mode of primordial gravitational waves [48, 49, 50]. Although, in practice, a large value of ε is required to falsify the possibility of an un-polarized GWB, combined results of the two different measurements lead to a valuable implication of the physics beyond standard inflationary predictions.

Acknowledgments

We would like to thank Eiichiro Komatsu for many helpful comments and discussions. We also thank Yasushi Suto, Shinji Mukohyama, Jun'ichi Yokoyama, Kazuhiro Yahata, Shun'ichiro Kinoshita, Takahiro Nishimichi, Yudai Suwa, and Erik Reese for useful discussions. K. I acknowledges the support from the Japan Society for Promotion of Science (JSPS) research fellows. A.T is supported by a Grant-in-Aid for Scientific Research from the JSPS (No.18740132).

Appendix A. CMB power spectra from tensor perturbation

In this appendix, we summarize the explicit form of the CMB power spectra for tensor modes. First write down the CMB power spectra as [28]:

$$C_\ell^{\mathrm{XY}(t)} = (4\pi)^2 \int k^2 dk P^t(k) \Delta^t_{\mathrm{X}\ell}(k) \Delta^t_{\mathrm{Y}\ell}(k) \; ; \quad (\mathrm{X,Y = T,E,B}), \tag{A.1}$$

where the photon transfer functions $\Delta^t_{\mathrm{X}\ell}(k)$ are the multipole moment of the function $\widetilde{\Delta}^t_X(k,\mu)$ (see below) and their explicit expressions are given by the integral form:

$$\Delta^t_{\mathrm{T}\ell}(k) = \sqrt{\frac{(\ell+2)!}{(\ell-2)!}}\int_0^{\eta_0} d\eta(-h'e^{-\tau}+g\Psi)P_{\mathrm{T}\ell}(x)\ , \tag{A.2}$$

$$\Delta^t_{\mathrm{E}\ell}(k) = \int_0^{\eta_0} d\eta(-g\Psi)P_{\mathrm{E}\ell}(x)\ , \tag{A.3}$$

$$\Delta^t_{\mathrm{B}\ell}(k) = \int_0^{\eta_0} d\eta(-g\Psi)P_{\mathrm{B}\ell}(x)\ , \tag{A.4}$$

with the quantity g being the visibility function defined by

$$g(\eta) = \tau'\,e^{-\tau}. \tag{A.5}$$

Here, τ is the optical depth for Thomson scattering between a given conformal time η and the present time η_0, the quantity h is the amplitude of the gravitational waves and $x \equiv k(\eta_0-\eta)$. The prime denotes the derivative with respect to the conformal time η, and the subscript t indicates the contribution from tensor modes. In the above expressions, the functions Ψ is the source function for radiative transfer of photon and $P_{\mathrm{E,B}\ell}$ are the projection factors for each polarization mode of photon, given by

$$\Psi \equiv \frac{1}{10}\widetilde{\Delta}^t_{\mathrm{T0}}+\frac{1}{7}\widetilde{\Delta}^t_{\mathrm{T2}}+\frac{3}{70}\widetilde{\Delta}^t_{\mathrm{T4}}-\frac{3}{5}\widetilde{\Delta}^t_{\mathrm{P0}}+\frac{6}{7}\widetilde{\Delta}^t_{\mathrm{P2}}-\frac{3}{70}\widetilde{\Delta}^t_{\mathrm{P4}}\ , \tag{A.6}$$

$$P_{\mathrm{T}\ell}(x) \equiv \frac{j_\ell(x)}{x^2}\ , \tag{A.7}$$

$$P_{\mathrm{E}\ell}(x) \equiv -j_\ell(x)+\partial_x^2 j_\ell(x)+\frac{2j_\ell(x)}{x^2}+\frac{4\partial_x j_\ell(x)}{x}\ , \tag{A.8}$$

$$P_{\mathrm{B}\ell}(x) \equiv 2\partial_x j_\ell(x)+\frac{4j_\ell(x)}{x}\ , \tag{A.9}$$

where $j_\ell(x)$ is the ℓ-th Bessel function. The expressions (A.1)–(A.9) are basically derived from the Boltzmann equations for photon's radiative transfer. To derive equations, first note that the quantities $\widetilde{\Delta}^t_X(k,\mu)$ are the solutions of the Boltzmann equation, which are formally written as the line-of-sight integral form:

$$\widetilde{\Delta}^t_{\mathrm{T}}(k,\mu) = \int_0^{\eta_0} d\eta\, e^{-ix\mu}(-h'\,e^{-\tau}+g\Psi), \tag{A.10}$$

$$\widetilde{\Delta}^t_{\mathrm{E}}(k,\mu) = \{-12+x^2(1-\partial_x^2)-8x\partial_x\}\widetilde{\Delta}^t_{\mathrm{P}}(k,\mu), \tag{A.11}$$

$$\widetilde{\Delta}^t_{\mathrm{B}}(k,\mu) = \{8x+2x^2\partial_x^2\}\widetilde{\Delta}^t_{\mathrm{P}}(k,\mu) \tag{A.12}$$

with the quantity $\widetilde{\Delta}^t_{\mathrm{P}}(k,\mu)$ being

$$\widetilde{\Delta}^t_{\mathrm{P}}(k,\mu) = \int_0^{\eta_0} d\eta\, e^{-ix\mu}(-g\Psi). \tag{A.13}$$

The quantities $\widetilde{\Delta}^t_X(k,\mu)$ are related to the direct observables of the temperature and the polarization maps, $X^t(\hat{n})$. Writing the projected maps as $X^t(\hat{n}) = \int d^3k\Delta^t_X(k,\hat{n})$, the relation between $\Delta^t_X(k,\hat{n})$ and $\widetilde{\Delta}^t_X(k,\mu)$ are given by

$$\Delta^t_{\mathrm{T}}(\mathbf{k},\hat{n}) = [(1-\mu^2)e^{2i\phi}\xi^{\mathrm{R}}(\mathbf{k})+(1-\mu^2)e^{-2i\phi}\xi^{\mathrm{L}}(\mathbf{k})]\widetilde{\Delta}^t_{\mathrm{T}}(k,\mu)\ , \tag{A.14}$$

$$\Delta^t_{\mathrm{E}}(\mathbf{k},\hat{n}) = [(1-\mu^2)e^{2i\phi}\xi^{\mathrm{R}}(\mathbf{k})+(1-\mu^2)e^{-2i\phi}\xi^{\mathrm{L}}(\mathbf{k})]\widetilde{\Delta}^t_{\mathrm{E}}(k,\mu)\ , \tag{A.15}$$

$$\Delta^t_{\mathrm{B}}(\mathbf{k},\hat{n}) = [-(1-\mu^2)e^{2i\phi}\xi^{\mathrm{R}}(\mathbf{k})+(1-\mu^2)e^{-2i\phi}\xi^{\mathrm{L}}(\mathbf{k})]\widetilde{\Delta}^t_{\mathrm{B}}(k,\mu)\ . \tag{A.16}$$

Here, the variables, $\xi^{\rm L,R}(\mathbf{k})$, are the independent random variables characterizing the statistical properties of the GWB. In this paper, we assume that

$$\langle \xi^{\rm L*}(\mathbf{k})\xi^{\rm L}(\mathbf{k}')\rangle = \delta(\mathbf{k}-\mathbf{k}')\, P^{t\rm L}(k)\ , \tag{A.17}$$

$$\langle \xi^{\rm R*}(\mathbf{k})\xi^{\rm R}(\mathbf{k}')\rangle = \delta(\mathbf{k}-\mathbf{k}')\, P^{t\rm R}(k)\ , \tag{A.18}$$

$$\langle \xi^{\rm L*}(\mathbf{k})\xi^{\rm R}(\mathbf{k}')\rangle = 0\ . \tag{A.19}$$

Starting from the line-of-sight integral solutions of the Boltzmann equation (A.10)–(A.12) and using the relations (A.14)–(A.19), one can derive the expressions for the CMB power spectra (A.1)–(A.2) with help of the definition (9) and the multipole expansion of the anisotropies on a projected sky:

$$a^{\rm X}_{\ell m} = \int d\Omega\ Y^*_{\ell m}(\hat{n}) \int d^3\mathbf{k}\ \Delta^t_{\rm X}(\eta_0,\mathbf{k},\hat{n})\ . \tag{A.20}$$

For details of the derivation, the readers may refer to Refs.[28, 52].

Appendix B. Linear polarization of the GWB and CMB power spectra

In this paper, we have mainly focused on the detectability of circularly polarized GWB. Here, we briefly discuss the measurability of a linearly polarized GWB.

Let us recall that the circularly polarized states of gravitational waves are related to the linearly polarized states as $h^L=(h^+ + ih^\times)/\sqrt{2}$ and $h^R=(h^+ - ih^\times)/\sqrt{2}$. Using this relationship, the power spectra of linearly polarized GWB can be rewritten with

$$\begin{aligned} P^{t+}(k) &= \langle \xi^{+*}\xi^{+}\rangle \\ &= \Big\langle (\xi^{\rm L*}+\xi^{\rm R*})(\xi^{\rm L}+\xi^{\rm R})\Big\rangle/2 \\ &= P^{t\rm C}(k) + \{P^{t\rm R}(k)+P^{t\rm L}(k)\}/2 \\ &= P^{t\rm C}(k) + P^{t}(k)/2\ , \end{aligned} \tag{B.1}$$

$$\begin{aligned} P^{t\times}(k) &= \Big\langle \xi^{\times *}\xi^{\times}\Big\rangle \\ &= \Big\langle (\xi^{\rm L*}-\xi^{\rm R*})(\xi^{\rm L}-\xi^{\rm R})\rangle/2 \\ &= -\,P^{t\rm C}(k) + \{P^{t\rm R}(k)+P^{t\rm L}(k)\}/2 \\ &= -\,P^{t\rm C}(k) + P^{t}(k)/2\ , \end{aligned} \tag{B.2}$$

where we have defined the cross power spectrum between left- and right-handed polarized states by $P^{t\rm C}(k)\equiv\langle\xi^{\rm L*}\xi^{\rm R}+\xi^{\rm R*}\xi^{\rm L}\rangle/2$. The above expressions readily imply that the linearly polarized GWB comes from the non-vanishing contribution of cross power spectrum $P^{t\rm C}(k)$. Thus, the crucial question is whether the cross power spectrum $P^{t\rm C}(k)$ is measurable or not.

To clarify this, consider the TT-mode power spectra. Following the definition (9), we have

$$\begin{aligned} C_\ell^{{\rm TT}(t)} &= \frac{1}{2\ell+1}\sum_m \langle a^{\rm T*}_{\ell m} a^{\rm T}_{\ell m}\rangle \\ &= \frac{1}{2\ell+1}\sum_m \int d\Omega' \int d\Omega \int d^3\mathbf{k}' \int d^3\mathbf{k}\ Y_{\ell m}(\hat{n}') Y^*_{\ell m}(\hat{n}) \\ &\qquad \times \Big\langle\ \Delta^{t*}_{\rm T}(\eta_0,\mathbf{k}',\hat{n}')\Delta^{t}_{\rm T}(\eta_0,\mathbf{k},\hat{n})\ \Big\rangle. \end{aligned} \tag{B.3}$$

from equation (A.20). The substitution of equation (A.14) into the above expression leads to

$$
\begin{aligned}
C_\ell^{\mathrm{TT}(t)} &= \frac{1}{2\ell+1}\sum_m \int d\Omega' \int d\Omega \int d^3\mathbf{k}' \int d^3\mathbf{k}\; Y_{\ell m}(\hat{n}')Y^*_{\ell m}(\hat{n}) \\
&\qquad \times \Big\langle (1-\mu'^2)\left\{e^{-2i\phi'}\xi^{\mathrm{R}*}(\mathbf{k}') + e^{2i\phi}\xi^{\mathrm{L}*}(\mathbf{k}')\right\}\widetilde{\Delta}^{t*}_{\mathrm{T}}(\eta_0,k') \\
&\qquad\quad \times (1-\mu^2)\left\{e^{2i\phi}\xi^{\mathrm{R}}(\mathbf{k}) + e^{-2i\phi}\xi^{\mathrm{L}}(\mathbf{k})\right\}\widetilde{\Delta}^{t}_{\mathrm{T}}(\eta_0,k)\Big\rangle \\
&= \frac{1}{2\ell+1}\sum_m \int d\Omega' \int d\Omega \int d^3\mathbf{k}' \int d^3\mathbf{k}\; Y_{\ell m}(\hat{n}')Y^*_{\ell m}(\hat{n}) \\
&\qquad \times (1-\mu'^2)(1-\mu^2)\widetilde{\Delta}^{t*}_{\mathrm{T}}(\eta_0,k')\widetilde{\Delta}^{t}_{\mathrm{T}}(\eta_0,k) \\
&\qquad \times \Big[(e^{2i\phi}e^{-2i\phi'} + e^{-2i\phi}e^{-2i\phi'})P^t(k)\delta(\mathbf{k}-\mathbf{k}')/2 \\
&\qquad\quad + \Big\langle e^{-2i\phi'}e^{-2i\phi}\xi^{R*}(\mathbf{k}')\xi^{L}(\mathbf{k}) + e^{2i\phi'}e^{2i\phi}\xi^{L*}(\mathbf{k}')\xi^{R}(\mathbf{k})\Big\rangle\Big] \;. \qquad \text{(B.4)}
\end{aligned}
$$

In the last line of equation (B.4), there appears the cross-correlation of the ensemble between ξ^L and ξ^R, which represents the contribution from the linearly polarized GWB. However, further proceeding to the integral over the azimuthal angle ϕ, it turns out that this term becomes vanishing. Because of $Y_{\ell m} \propto e^{im\phi}$, the relevant part of the integral over ϕ can be written as

$$\int_0^{2\pi} d\phi e^{\pm 2i\phi}e^{-im\phi} = 2\pi\delta_{m\pm2} \;, \qquad \text{(B.5)}$$

which thus leads to

$$\left(\int_0^{2\pi} d\phi' e^{2i\phi'}e^{im\phi'}\right)\left(\int_0^{2\pi} d\phi e^{2i\phi}e^{-im\phi}\right) = (2\pi)^2\delta_{m2}\delta_{m-2} = 0 \;. \qquad \text{(B.6)}$$

Hence, linearly polarized GWB is shown to be null effect on the TT-mode power spectrum. Note that similar argument does hold for the other power spectra, since all of the photon transfer functions Δ^t_{X} are written by a linear combination of $e^{2i\,\phi}\xi^{\mathrm{R}}$ and $e^{-2i\,\phi}\xi^{\mathrm{L}}$ (see Eqs.(A.14), (A.15) and (A.16)). Thus, the cross correlation term always has the factor $e^{-2i\phi'}e^{-2i\phi}$ or $e^{2i\phi'}e^{2i\phi}$, which finally vanishes after the integration over the azimuthal angle.

Appendix C. Characteristic features of TB- and EB-mode power spectra

In this appendix, we discuss the details in characteristic features of TB- and EB-mode power spectra originating from circularly polarized GWB.

§4.1 reveals that while the TB-mode power spectrum has one zero-crossing point around $\ell \sim 70$, the EB-mode power spectrum has many zero-crossing points with tiny amplitudes. These features are mainly attributed to the projection factors in photon's transfer function, $\Delta^t_{\mathrm{T,E,B}\ell}$ (see (A.7)-(A.9)).

$$
\begin{aligned}
P_{\mathrm{T}\ell}(x) &\equiv \frac{j_\ell(x)}{x^2} \;, \\
P_{\mathrm{E}\ell}(x) &\equiv -j_\ell(x) + \partial_x^2 j_\ell(x) + \frac{2j_\ell(x)}{x^2} + \frac{4\partial_x j_\ell(x)}{x} \;,
\end{aligned}
$$

$$P_{\mathrm{B}\ell}(x) \equiv 2\partial_x j_\ell(x) + \frac{4j_\ell(x)}{x} \ ,$$

Let us first consider the TB-mode spectrum, in which there appears the projection factors, $P_{\mathrm{T}\ell}(x)\times P_{\mathrm{B}\ell}(x)$, in the kernel of the integral (A.1). Figure C1 shows the function, $P_{\mathrm{T}\ell}(x) \times P_{\mathrm{B}\ell}(x)$, as function of $x = k(\eta_0 - \eta)$ for various multipoles with $\ell = 10$ (*top*), 70 (*middle*) and 100 (*bottom*). The function starts to oscillate around $x \sim \ell$ and it asymptotically decays as x^{-4}. Thus, the main contribution to the integral in equation (A.1) comes from the first several peaks in the oscillations and many oscillations at large x are almost canceled out. Just focusing on the first part around $x \sim \ell$, we find that the positive part of the oscillating amplitudes has relatively larger values for lower-multipoles, while the amplitude at higher-multipoles has slightly large negative amplitudes. Eventually, the values of the positive and negative amplitudes become comparable at the multipole $\ell \sim 70$. These behaviors quantitatively explain the shape of the TB-mode power spectrum.

Similarly, tiny amplitude of the EB-mode spectrum is also explained by the projection factor, $P_{\mathrm{E}\ell}(x)$ and $P_{\mathrm{B}\ell}(x)$. In Figure C2, we plot the projection factor of EB-mode power spectrum, $P_{\mathrm{E}\ell}(x) \times P_{\mathrm{B}\ell}(x)$ (*blue dot*), together with those of the BB- and EE-mode spectra, $P_{\mathrm{B}\ell}(x)^2$ (*green, short-dashed*) and $P_{\mathrm{E}\ell}(x)^2$ (*red, solid*). The oscillation of the projection factor $P_{\mathrm{B}\ell}(x)^2$ is $\pi/2$ out of phase with corresponding one of EE-mode power spectrum. Thus, the amplitude of the product, $P_{\mathrm{E}\ell}(x) \times P_{\mathrm{B}\ell}(x)$, is degraded as a result of phase cancellation. Hence, the amplitude of EB-mode power spectrum becomes much smaller than those of the EE- and BB-mode spectra.

Appendix D. Weak lensing effect on CMB power spectra

Here, we derive the expression for the lensed TB-mode power spectrum following the discussion in Ref.[43]. The gravitational lensing effect appears as the angular excursion of the photon path. Since the lensing effect is only relevant at the small angular scales in the CMB, we consider the small scale limit. In terms of Fourier components we have following the expressions for the Stokes parameters:

$$\begin{aligned} T(\vec{\theta}) &= \widetilde{T}(\vec{\theta}+\delta\vec{\theta}) = \int \frac{d^2\vec{\ell}}{(2\pi)^2} e^{i\vec{\ell}\cdot(\vec{\theta}+\delta\vec{\theta})} T(\vec{\ell}) \ , \\ Q(\vec{\theta}) &= \widetilde{Q}(\vec{\theta}+\delta\vec{\theta}) = \int \frac{d^2\vec{\ell}}{(2\pi)^2} e^{i\vec{\ell}\cdot(\vec{\theta}+\delta\vec{\theta})} Q(\vec{\ell}) \ , \\ U(\vec{\theta}) &= \widetilde{U}(\vec{\theta}+\delta\vec{\theta}) = \int \frac{d^2\vec{\ell}}{(2\pi)^2} e^{i\vec{\ell}\cdot(\vec{\theta}+\delta\vec{\theta})} U(\vec{\ell}) \ , \end{aligned} \tag{D.1}$$

where $\widetilde{X}$ describes the unlensed X.

The polarization parameter Q and U can be expressed with E and B as:

$$\begin{aligned} Q(\vec{\ell}) &= E(\vec{\ell})\cos 2\phi_\ell - B(\vec{\ell})\sin 2\phi_\ell \ , \\ U(\vec{\ell}) &= E(\vec{\ell})\sin 2\phi_\ell + B(\vec{\ell})\cos 2\phi_\ell \ , \end{aligned} \tag{D.2}$$

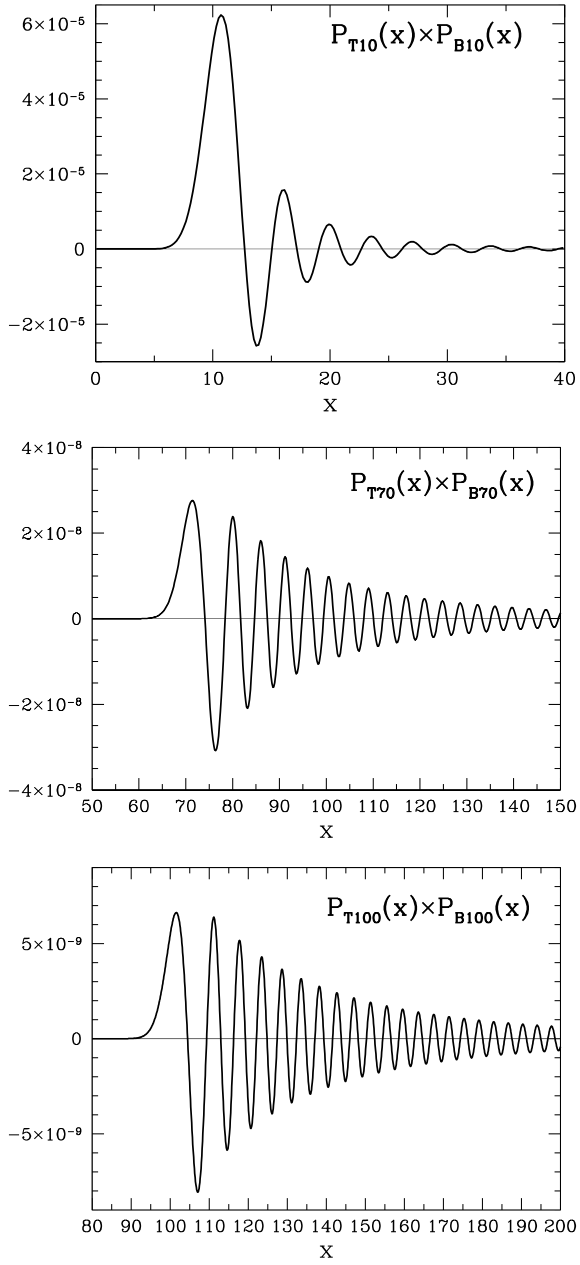

Figure C1. The projection factor of TB-mode spectrum, $P_{\mathrm{T}\ell}(x) \times P_{\mathrm{B}\ell}(x)$, as function of $x = k(\eta_0 - \eta)$. The *top*, *middle*, and *bottom* panels represent the results with multipoles $\ell = 10$, $\ell = 70$, and $\ell = 100$, respectively.

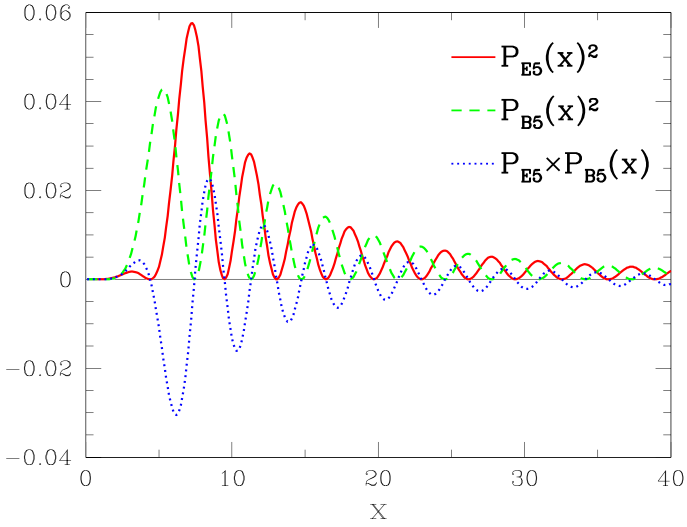

Figure C2. The projection factors of EE-, BB- and EB-mode power spectra at the multipole $\ell = 5$: $P_{\mathrm{E}\ell}(x)^2$(*red, solid*), $P_{\mathrm{B}\ell}(x)^2$(*green, short-dash*), and $P_{\mathrm{E}\ell}(x) \times P_{\mathrm{B}\ell}(x)$(*blue, dot*).

where ϕ_ℓ is the azimuthal angle. The ensemble average of each Fourier components becomes

$$\langle \widetilde{X}(\vec{\ell})\widetilde{Y}(\vec{\ell}')\rangle = (2\pi)^2 C_\ell^{\widetilde{\mathrm{X}}\widetilde{\mathrm{Y}}}\delta(\vec{\ell}-\vec{\ell}') \tag{D.3}$$

with $\widetilde{X}, \widetilde{Y} = \widetilde{T}, \widetilde{E}$ and $\widetilde{B}$. Using equations (D.1), (D.2) and (D.3), cross correlation functions C_{TQ} and C_{TU} are expressed as

$$C_{\mathrm{TQ}}(\theta) = \int \frac{d^2\vec{\ell}}{(2\pi)^2} e^{i\ell\theta\cos\phi_\ell}\langle e^{i\vec{\ell}\cdot(\delta\vec{\theta}_A-\delta\vec{\theta}_B)}\rangle[C_\ell^{\widetilde{\mathrm{T}}\widetilde{\mathrm{E}}}\cos 2\phi_\ell - C_\ell^{\widetilde{\mathrm{T}}\widetilde{\mathrm{B}}}\sin 2\phi_\ell],$$

$$C_{\mathrm{TU}}(\theta) = \int \frac{d^2\vec{\ell}}{(2\pi)^2} e^{i\ell\theta\cos\phi_\ell}\langle e^{i\vec{\ell}\cdot(\delta\vec{\theta}_A-\delta\vec{\theta}_B)}\rangle[C_\ell^{\widetilde{\mathrm{T}}\widetilde{\mathrm{E}}}\sin 2\phi_\ell - C_\ell^{\widetilde{\mathrm{T}}\widetilde{\mathrm{B}}}\cos 2\phi_\ell], \tag{D.4}$$

where we set θ as $\theta \equiv \theta_A - \theta_B$. The above expressions still possess the ensemble average, which represents the statistical average over the photon excursions caused by the lensing effect. In the weak lensing limit, the angular excursion is approximately described by the random Gaussian distribution with small dispersion. We have (e.g., Ref.[51]):

$$\begin{aligned}\langle e^{i\vec{\ell}\cdot(\delta\vec{\theta}_A-\delta\vec{\theta}_B)}\rangle &= \exp\left\{-\frac{\ell^2}{2}[\sigma_0^2(\theta)+\cos(2\phi_\ell)\sigma_2^2(\theta)]\right\} \\ &\simeq 1-\frac{\ell^2}{2}[\sigma_0^2(\theta)+\cos(2\phi_\ell)\sigma_2^2(\theta)] \ .\end{aligned} \tag{D.5}$$

The functions, σ_0^2 and σ_2^2, characterize the rms fluctuations of the photon path (see Ref.[43] for their explicit expressions). Substituting the relation (D.5) into (D.4) and integrating over the azimuthal angle ϕ_ℓ, we obtain

$$C_{\mathrm{TQ}}(\theta) = -\int \frac{\ell d\ell}{2\pi} C_\ell^{\widetilde{\mathrm{T}}\widetilde{\mathrm{E}}}\left[J_2(\ell\theta)\left\{1-\frac{\ell^2\sigma_0^2(\theta)}{2}\right\}+\frac{\ell^2\sigma_2^2(\theta)}{4}\{J_0(\ell\theta)+J_4(\ell\theta)\}\right] \ ,$$

$$C_{\rm TU}(\theta) = -\int \frac{\ell d\ell}{2\pi} C_\ell^{\widetilde{\rm T}\widetilde{\rm B}} \left[J_2(\ell\theta) \left\{ 1 - \frac{\ell^2\sigma_0^2(\theta)}{2} \right\} + \frac{\ell^2\sigma_2^2(\theta)}{4} \left\{ J_0(\ell\theta) + J_4(\ell\theta) \right\} \right] . \tag{D.6}$$

The above expressions finally lead to the angular power spectrum of TB mode with a help of the relation:

$$C_\ell^{\rm TB} = -2\pi \int_0^\pi \theta d\theta C_{\rm TU}(\theta) J_2(\ell\theta) \ , \tag{D.7}$$

The resultant expression becomes

$$C_\ell^{\rm TB} = C_\ell^{\widetilde{\rm T}\widetilde{\rm B}} + \sum_{\ell'} \mathcal{W}_\ell^{\ell'} C_{\ell'}^{\widetilde{\rm T}\widetilde{\rm B}} \ , \tag{D.8}$$

$$\mathcal{W}_\ell^{\ell'} \ = \int_0^\pi \theta d\theta J_2(\ell\theta) \left[-\frac{\ell'^3}{2}\sigma_0^2(\theta) J_2(\ell'\theta) + \frac{\ell'^3}{4}\sigma_2^2(\theta) \{ J_0(\ell'\theta) + J_4(\ell'\theta) \} \right] . \tag{D.9}$$

That is, the lensed power spectrum of the TB-mode is generated if and only if the primary TB-mode exists. No other cross spectra can create the lensed TB-mode. This may be explained intuitively by a simple symmetry reason; the change of TE-mode into TB-mode breaks parity which we do not expect from weak lensing effect. Since the transformation matrix $\mathcal{W}_\ell^{\ell'}$ is the oscillating function whose amplitude is basically much less than unity [43], the lensing effect on the TB-mode spectrum can be safely neglected as long as the primary TB-mode spectrum is generated from the tensor-type fluctuations.

Appendix E. Exact form of likelihood function

In this Appendix, we briefly sketch the derivation of the exact likelihood function used in §5.2. To do this, we first follow the simplest case of the likelihood function with temperature anisotropy data alone. The likelihood function for the temperature anisotropies observed by a perfect experiment (i.e., noiseless and full-sky observation) has the following form:

$$\mathcal{L}(\vec{T}|\bar{C}_\ell^{\rm TT}) \propto \frac{1}{\sqrt{|\mathbf{S}|}} \exp\left[-\frac{\vec{T}^{\rm T}\mathbf{S}^{-1}\vec{T}}{2} \right] \ , \tag{E.1}$$

where $\vec{T}$ denotes our temperature map, $\mathbf{S}$ is correlation matrix given by $S_{ij} = \sum_\ell (2\ell + 1)\overline{C}_\ell^{\rm TT} P_\ell(\hat{n}_i \cdot \hat{n}_j)/(4\pi)$, where the P_ℓ are the Legendre polynomials and $\hat{n}_i$ is the pixel position on the map, and $|\mathbf{S}|$ denotes determinant of correlation matrix. Expanding the temperature map in spherical harmonics: $T(\hat{n}) = \sum_{\ell m} a_{\ell m}^{\rm T} Y_{\ell m}(\hat{n})$, the likelihood function for each $a_{\ell m}^{\rm T}$ becomes

$$\mathcal{L}(\vec{T}|\overline{C}_\ell^{\rm TT}) \propto \prod_{\ell m} \frac{1}{\sqrt{\bar{C}_\ell^{\rm TT}}} \exp\left(-\frac{|a_{\ell m}^{\rm T}|^2}{2\overline{C}_\ell^{\rm TT}} \right) . \tag{E.2}$$

If we assume that each multipole moment $a_{\ell m}^{\rm T}$ just follows the Gaussian statistics with variance of $\bar{C}_\ell^{\rm TT}$, the above expression can be reduced to aχ^2-distribution with $(2\ell+1)$ degrees of freedom:

$$-2\ln\mathcal{L}=\sum_\ell\left[-(2\ell-1)\ln\widehat{C}_\ell^{\rm TT}+(2\ell+1)\left(\ln\overline{C}_\ell^{\rm TT}+\frac{\widehat{C}_\ell^{\rm TT}}{\overline{C}_\ell^{\rm TT}}-1\right)\right],\tag{E.3}$$

where $\widehat{C}_\ell^{\rm TT}$ denotes the estimator defined by $\widehat{C}_\ell^{\rm TT}=\sum_m|a_{\ell m}^{\rm T}|^2/(2\ell+1)$.

Assuming a uniform prior distribution, the posterior distribution function is proportional to the likelihood function as a result of Bayes' theorem. Thus, the likelihood function (E.3) can be viewed as the posterior distribution function, as a function of the theoretical value, $\overline{C}_\ell^{\rm TT}$. Then, appropriately normalizing the posterior distribution, the exact expression of the likelihood function for temperature anisotropy data is obtained:

$$-2\ln\mathcal{L}(\overline{C}_\ell^{\rm TT})=\sum_\ell(2\ell+1)\left[\ln\left(\frac{\overline{C}_\ell^{\rm TT}}{\widehat{C}_\ell^{\rm TT}}\right)+\frac{\widehat{C}_\ell^{\rm TT}}{\overline{C}_\ell^{\rm TT}}-1\right].\tag{E.4}$$

The above result can be extended to the likelihood functions for the general case with temperature and polarization anisotropies. Restricting the analysis to the case of the temperature and B-mode polarization data, the likelihood function becomes

$$\mathcal{L}=\prod_{\ell m}\frac{1}{\sqrt{|\mathbf{C}|}}\exp\left[-\frac{\vec{d}^T\mathbf{C}^{-1}\vec{d}}{2}\right],\tag{E.5}$$

where the vector $\vec{d}$ and the matrix $\mathbf{C}$ are respectively given by

$$\vec{d}^{\rm T}=(a_{\ell m}^{\rm T},a_{\ell m}^{\rm B}),\tag{E.6}$$

$$\mathbf{C}=\begin{pmatrix}\overline{C}_\ell^{\rm TT} & \overline{C}_\ell^{\rm TB}\\ \overline{C}_\ell^{\rm TB} & \overline{C}_\ell^{\rm BB}\end{pmatrix}.\tag{E.7}$$

Then, just repeating the same procedure as presented above, we obtain the likelihood function:

$$\begin{aligned}-2\ln\mathcal{L}=\sum_\ell(2\ell+1)&\left\{\ln\left(\frac{\overline{C}_\ell^{\rm TT}\overline{C}_\ell^{\rm BB}-(\overline{C}_\ell^{\rm TB})^2}{\widehat{C}_\ell^{\rm TT}\widehat{C}_\ell^{\rm BB}-(\widehat{C}_\ell^{\rm TB})^2}\right)\right.\\&\left.+\frac{\widehat{C}_\ell^{\rm TT}\overline{C}_\ell^{\rm BB}+\overline{C}_\ell^{\rm TT}\widehat{C}_\ell^{\rm BB}-2\overline{C}_\ell^{\rm TB}\widehat{C}_\ell^{\rm TB}}{\overline{C}_\ell^{\rm TT}\overline{C}_\ell^{\rm BB}-(\overline{C}_\ell^{\rm TB})^2}-2\right\}.\end{aligned}\tag{E.8}$$

Reference

[1] J. Bock *et al.*, arXiv:astro-ph/0604101.

[2] L. Verde, H. Peiris and R. Jimenez, JCAP **0601**, 019 (2006) [arXiv:astro-ph/0506036].

[3] A. Amblard, A. Cooray and M. Kaplinghat, Phys. Rev. D **75**, 083508 (2007) [arXiv:astro-ph/0610829].

[4] A. Cooray, Mod. Phys. Lett. **20** 2503 (2005) [arXiv:astro-ph/0503118].

[5] T. L. Smith, M. Kamionkowski and A. Cooray, Phys. Rev. D **73**, 023504 (2006) [arXiv:astro-ph/0506422].

[6] T. L. Smith, H. V. Peiris and A. Cooray, Phys. Rev. D **73**, 123503 (2006) [arXiv:astro-ph/0602137].

[7] H. Kudoh, and A. Taruya, T. Hiramatsu and Y. Himemoto, Phys. Rev. D **73**, 064006 (2006) [arXiv:gr-qc/0511145].

[8] E. Phinney et al, NASA Mission Concept Study (2003).

[9] N. Seto, S. Kawamura and T. Nakamura, Phys. Rev. Lett. **87**, 221103 (2001) [arXiv:astro-ph/0108011].

[10] S. Kawamura, et al., Class. Quant. Grav. **23**, 125 (2006)

[11] M. Green and J. Shwarz Phys. Lett. B **149**, 117 (1984) .

[12] E. Witten Phys. Lett. B **149**, 351 (1984) .

[13] A. Lue, L. M. Wang and M. Kamionkowski, Phys. Rev. Lett. **83**, 1506 (1999) [arXiv:astro-ph/9812088].

[14] K. Choi, J. c. Hwang and K. W. Hwang, Phys. Rev. D **61**, 084026 (2000) [arXiv:hep-ph/9907244].

[15] R. Jackiw and S. Y. Pi, Phys. Rev. D **68**, 104012 (2003) [arXiv:gr-qc/0308071].

[16] D. H. Lyth, C. Quimbay and Y. Rodriguez, JHEP **0503**, 016 (2005) [arXiv:hep-th/0501153].

[17] S. Alexander and J. Martin, Phys. Rev. D **71**, 063526 (2005) [arXiv:hep-th/0410230].

[18] S. Alexander, M. Peskin and M. Sheikh-Jabbari Phys. Rev. Lett. **96**, 081301 (2006) .

[19] S. Alexander and S. Gates Jr. JCAP **06**, 018 (2006) .

[20] M. Satoh, S. Kanno and J. Soda, arXiv:0706.3585 [astro-ph].

[21] I. Antoniadis, J. Rizos and K. Tamvakis, Nucl. Phys. B **415**, 497 (1994) [arXiv:hep-th/9305025].

[22] R. Brustein and R. Madden, JHEP **9907**, 006 (1999) [arXiv:hep-th/9901044].

[23] C. Caprini, R. Durrer and T. Kahniashvili, Phys. Rev. D **69**, 063006 (2004) [arXiv:astro-ph/0304556].

[24] T. Kahniashvili, G. Gogoberidze and B. Ratra, Phys. Rev. Lett. **95**, 151301 (2005) [arXiv:astro-ph/0505628].

[25] D. N. Spergel *et al.* [WMAP Collaboration], arXiv:astro-ph/0603449.

[26] L. Page *et al.* [WMAP Collaboration], arXiv:astro-ph/0603450.

[27] R. Brustein and D. H. Oaknin, Phys. Rev. Lett. **82**, 2628 (1999) [arXiv:hep-ph/9809365].

[28] M. Zaldarriaga and U. Seljak, Phys. Rev. D **55**, 1830 (1997) [arXiv:astro-ph/9609170].

[29] M. Kamionkowski, A. Kosowsky and A. Stebbins, Phys. Rev. D **55**, 7368 (1997) [arXiv:astro-ph/9611125].

[30] W. Hu and M. J. White, Phys. Rev. D **56**, 596 (1997) [arXiv:astro-ph/9702170].

[31] B. Feng, M. Li, J. Q. Xia, X. Chen and X. Zhang, Phys. Rev. Lett. **96**, 221302 (2006) [arXiv:astro-ph/0601095].

[32] G. C. Liu, S. Lee and K. W. Ng, Phys. Rev. Lett. **97**, 161303 (2006) [arXiv:astro-ph/0606248].

[33] P. Cabella, P. Natoli and J. Silk, arXiv:0705.0810 [astro-ph].

[34] E. S. Scannapieco and P. G. Ferreira, Phys. Rev. D **56**, 7493 (1997) [arXiv:astro-ph/9707115].

[35] A. Kosowsky and A. Loeb, Astrophys. J. **469**, 1 (1996) [arXiv:astro-ph/9601055].

[36] J. R. Pritchard and M. Kamionkowski, Annals Phys. **318**, 2 (2005) [arXiv:astro-ph/0412581].

[37] Y. Zhang, W. Zhao, T. Xia and Y. Yuan, Phys. Rev. D **74**, 083006 (2006) [arXiv:astro-ph/0508345].

[38] A. Lewis, A. Challinor and A. Lasenby, Astrophys. J. **538**, 473 (2000) [arXiv:astro-ph/9911177].

[39] X. H. Fan, C. L. Carilli and B. Keating, Ann. Rev. Astron. Astrophys. **44**, 415 (2006) [arXiv:astro-ph/0602375].

[40] M. M. Basko and A. G.Polnarev, Mon. Not. Roy. Astron. Soc. **191**, 207 (1980).

[41] M. Zaldarriaga, Phys. Rev. D **55**, 1822 (1997) [arXiv:astro-ph/9608050].

[42] A. Lewis and A. Challinor, Phys. Rept. **429**, 1 (2006) [arXiv:astro-ph/0601594].

[43] M. Zaldarriaga and U. Seljak, Phys. Rev. D **58**, 023003 (1998) [arXiv:astro-ph/9803150].

[44] Planck Collaboration, "Planck: The scientific programme," arXiv:astro-ph/0604069.

[45] A. Lewis and S. Bridle, Phys. Rev. D **66**, 103511 (2002) [arXiv:astro-ph/0205436].

[46] J. R. Bond, A. H. Jaffe and L. E. Knox, Astrophys. J. **533**, 19 (2000) [arXiv:astro-ph/9808264].

[47] L. Perotto, J. Lesgourgues, S. Hannestad, H. Tu, Y.Y.Y Wong, JCAP **10**, 013 (2006) [arXiv:astro-ph/0606227].

[48] N. Seto, Phys. Rev. Lett. **97**, 151101 (2006) [arXiv:astro-ph/0609504].

[49] N. Seto, Phys. Rev. D **75**, 061302 (2007) [arXiv:astro-ph/0609633].
[50] N. Seto and A. Taruya, Phys. Rev. Lett. in press (2007)
[51] U. Seljak, Astrophys. J. **463**, 1 (1996) [arXiv:astro-ph/9505109].
[52] Y.T. Lin, D. Wandelt, Astropart. Phys. **25**, 151 (2006) [arXiv:astro-ph/0409734].